Article

Preparation and Capacitive Properties of Ni-Doped Zinc Cobaltate/Carbon Fiber Composite Porous Mesh Materials

Donghua Chen [1],*, Yang Liu [1], Jun Wang [1], Tenghao Ma [1], Hui Zhi [1], Wei Xiao [1], Yabin Wang [2] and Jing Wang [1]

[1] School of Light Industry, Harbin University of Commerce, Harbin 150028, China; ly760576542@163.com (Y.L.); wangjun1003@163.com (J.W.); 18234590846@163.com (T.M.); 102618@hrbcu.edu.cn (H.Z.); xiaoweianny@126.com (W.X.); wangwangmayong@126.com (J.W.)

[2] College of Chemistry and Chemical Engineering, Yan'an University, Yan'an 716000, China; ybw@yau.edu.cn

* Correspondence: 102959@hrbcu.edu.cn

Abstract: Nickel-element-doped zinc cobaltate/carbon fiber composites (Ni-ZnCo$_2$O$_4$/CF) were prepared on carbon cloth (made of a combination of carbon fibers) conductive substrates using a simple ambient stirring method combined with heat treatment. Characterization tests of the materials revealed that the prepared products were porous Ni-ZnCo$_2$O$_4$/CF mesh structures. This porous network structure increases the surface area of the material and helps shorten the diffusion path of ions and electrons. The samples were analyzed using X-ray diffraction (XRD), scanning electron microscopy (SEM), and transmission electron microscopy (TEM) methods to investigate the effect of Ni elemental doping on the stability of the materials. The results show that there are no other impurity peaks and no other impurity elements in the Ni-ZnCo$_2$O$_4$/CF electrode material, which indicates that the sample purity is high. Meanwhile, the electrochemical properties of Ni-ZnCo$_2$O$_4$/CF electrode materials were studied. Under the condition of 15 A·g^{-1}, the specific capacitance of Ni-ZnCo$_2$O$_4$/CF electrode material is 1470 F·g^{-1}, and after 100 cycles, its specific capacity reaches 1456 F·g^{-1}, which is 99.0% of the specific capacity of 1470 F·g^{-1}, indicating that the electrode material has good stability. In addition, we assembled asymmetric supercapacitors (Ni-ZnCo$_2$O$_4$/CF//CNTs) with Ni-ZnCo$_2$O$_4$/CF as the positive material and carbon nanotubes (CNTs) as the negative material. In the cyclic stability experiment of Ni-ZnCo$_2$O$_4$/CF/CNTs devices, when the current density was 1 A·g^{-1}, the specific capacitance was 182 F·g^{-1}. After 10,000 cyclic charge–discharge tests, the specific capacity became 167 F·g^{-1}, which was basically unchanged compared with the initial specific capacity, reaching 91.8%. It shows that it has higher charge–discharge performance and higher cycle stability.

Keywords: zinc cobaltate; electrodes; mixing method at room temperature; composite material; ultra-capacitor

1. Introduction

At the same time as rapid industrial development, problems such as environmental pollution and energy supply shortage have caused great inconvenience to people's production and life [1]. Electricity is an economical, practical, clean, easy-to-control and -convert energy, which is suitable for a variety of environments. However, electricity has the fatal disadvantage of being difficult to store. In order to realize the effective storage and use of energy, it is necessary to design an energy storage device with high efficiency and high stability [2]. Supercapacitors have the advantages of long service life, high power density, fast charging speed, and environmental protection [3]. At the same time, water pollution is also a major environmental problem currently being faced; rational use of light energy to achieve efficient degradation of organic matter in water can not only solve the energy crisis but can also effectively protect the environment. Therefore, there is an urgent need to develop new photocatalytic materials with good electrochemical properties and high efficiency. The microstructure of the material has an important effect on its electrochemical performance and catalytic activity [4,5].

Bimetallic oxide materials have high electrical conductivity, high theoretical specific capacity, good oxidation–reduction reversibility and high specific capacity [6,7]. Among them, zinc cobaltate ($ZnCo_2O_4$) is considered to be a potential supercapacitor electrode material because of its excellent electrochemical performance, high conductivity, low price, and green environmental protection characteristics, but its specific capacity and energy storage performance still need to be improved. By doping Ni elements, not only can this process improve its specific capacity, but it can also effectively store electrical energy and will not reduce its service life and conductivity.

In this paper, nickel-doped zinc cobaltate composites (Ni-$ZnCo_2O_4$/CF) with a porous network structure were synthesized on carbon cloth (made of a combination of carbon fibers) by the room-temperature stirring method combined with heat treatment. These materials have abundant pore structures, which are favorable for the transport of ions and electrons in the electrolyte. The results show that the synthesized cobalt cobaltate has a homogeneous network structure without other impurity peaks and high purity. The specific capacitance of Ni-$ZnCo_2O_4$/CF was 1470 $F \cdot g^{-1}$ at a current density of 15 $A \cdot g^{-1}$ and was 99.0% of the initial specific capacity after 100 changes. The prepared Ni-$ZnCo_2O_4$/CF materials were also assembled into asymmetric supercapacitor devices (Ni-$ZnCo_2O_4$/CF//CNTs) by using the prepared Ni-$ZnCo_2O_4$/CF materials as the anode materials and carbon nanotubes (CNTs) as the anode materials. The specific capacity of Ni-$ZnCo_2O_4$/CF//CNTs reaches 182 $F \cdot g^{-1}$ at a current density of 1 $A \cdot g^{-1}$, and after 10,000 charge/discharge tests, its specific capacity becomes 91.8% of the original one, which shows that the prepared material has good cycling performance and good cycle stability during the charging and discharging process.

2. Materials and Methods

2.1. Instruments

In this experiment, a scanning electron microscope (SEM, model S4800, acceleration voltage 0.1~30 kv, magnification 20×~800,000×,) and a transmission electron microscope (TEM, JEM-2100F) were used to observe the micro-morphology of the samples. The phase structure of the prepared materials was analyzed by X-ray diffractometer (XRD, XRD-700). The components of the prepared samples were analyzed by X-ray energy-dispersive spectrometry (EDS, JEM-2100Plus), a multi-channel workstation (1470E CellTest), and an electrochemical impedance test system (LEIS370/470). The samples required for experimental preparation are shown in Table 1.

Table 1. List of raw materials used in these experiments.

Drug Names	Molecular Formula	Manufacturer
Zinc Nitrate Hexahydrate	$Zn(NO_3)_2 \cdot 6H_2O$	Shanghai Aladdin Biochemical Technology Co., Ltd. (Shanghai, China)
Cobaltous nitrate hexahydrate	$Co(NO_3)_2 \cdot 6H_2O$	Tianjin Hiens Opdex Technology Co., Ltd. (Tianjin, China)
Ammonium fluoride	NH_4F	Langfang Qianyao Chemical Reagent Co., Ltd. (Langfang, China)
Urea	CH_4N_2O	Anhui Haoyuan Chemical Group Co., Ltd. (Fuyang, China)
Carbon cloth	C	Jiangsu Sutong Carbon Fiber Co., Ltd. (Nantong, China)
carbon nanotube	C	Jiangsu Cnano Technology Co., Ltd. (Zhenjiang, China)
Nickel nitrate hexahydrate	$Ni(NO_3)_2 \cdot 6H_2O$	Nanjing Chemical Reagent Co., Ltd. (Nanjing, China)

2.2. Preparation of $ZnCo_2O_4$

Firstly, 3.5 mmol of $Zn(NO_3)_2 \cdot 6H_2O$ was dissolved in 45 mL of deionized water. Then, 2 mmol of $Co(NO_3)_2 \cdot 6H_2O$, 2 mmol of NH_4F, and 4 mmol of urea were gradually added into the solution. At the same time, 1 cm^2 of carbon cloth (carbon fiber combination) conductive substrate was added. Use a magnetic stirrer to stir for 5 h, remove and prepare the sample, and then wash it repeatedly with anhydrous ethanol and deionized water. The precursor $ZnCo_2O_4$/CF was obtained by transferring the cleaned sample to the oven for drying at 50 °C for 5 h. Finally, $ZnCo_2O_4$/CF electrode materials were obtained by placing

$ZnCo_2O_4$/CF precursor in a Muffle furnace and heating at room temperature to 400 °C for 2 h.

2.3. Preparation of Ni-ZnCo₂O₄/CF Materials

The $ZnCo_2O_4$/CF material obtained above was dissolved in 45 mL of deionized water, and the $Ni(NO_3)_2 \cdot 6H_2O$ solution was added to the solution drop by drop, stirring for 3 h with a magnetic agitator, taking out the sample for preparation, and then washing repeatedly with anhydrous ethanol and deionized water. The precursor of Ni-$ZnCo_2O_4$/CF was obtained by transferring the cleaned sample to the oven for drying at 50 °C for 4 h. Finally, Ni-$ZnCo_2O_4$/CF electrode material was obtained by placing the precursor in a Muffle furnace at room temperature to 400 °C for 2 h. The preparation of porous Ni-$ZnCo_2O_4$/CF in the experiment is shown in Figure 1.
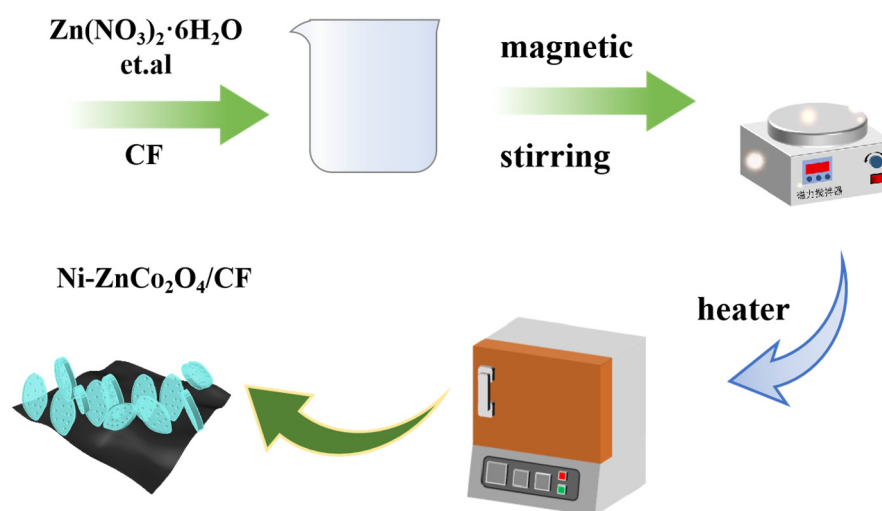

Figure 1. Schematic diagram of the preparation process of porous Ni-$ZnCo_2O_4$/CF material.

2.4. Nitrogen Adsorption and Desorption Test

A 500 mg amount of the sample to be tested was loaded into the sample tube, and the sample tube was loaded into the degassing station. Then, put the heating pack on the sample tube, turn on the vacuum pump, and start to evacuate the sample for 30 min. Next, turn on the heating switch and heat it for 5 h in order to remove the gas adsorbed on the surface of the material. After the degassing was finished, the heating power was turned off and the sample was cooled to room temperature and then backfilled with helium. After filling the sample with helium at atmospheric pressure, the sample tube was removed and immediately capped with a rubber stopper, weighed, and recorded. Load the weighed tubes into the analyzer station. Liquid nitrogen is added to the Dewar's flask, and the calculated sample mass is entered into the analytical file to begin adsorption and desorption testing.

2.5. Assembly of Asymmetric Supercapacitors

Assembly of asymmetric electrochemical capacitors: Porous Ni-$ZnCo_2O_4$/CF/CNTs asymmetric devices were prepared by using porous Ni-$ZnCo_2O_4$/CF composite material as the positive electrode, carbon nanotubes (CNTs) as the negative electrode, KOH as the electrolyte, and a diaphragm between the positive and negative electrodes. The relevant calculation formulas are as follows:

$$C_S = {i\Delta t} / {m\Delta V} \tag{1}$$

$$E = 0.5 C_S \Delta V^2 \tag{2}$$

$$P = 3600E \Big/ \Delta t \tag{3}$$

$$q = C_S \Delta V m \tag{4}$$

$$m^+ \Big/ m^- = C^- \Delta V^- \Big/ C^+ \Delta V^+ \tag{5}$$

where: C_S (specific capacity, F·g^{-1}); Δt (discharge time, s); m (mass of active material, g); E (Energy density, W·h·kg^{-1}); P (Power density, W·kg^{-1}).

3. Results and Discussion

Figure 2a,b are SEM images of Ni-ZnCo$_2$O$_4$/CF materials at different magnifications. It was observed by scanning electron microscope that the Ni-ZnCo$_2$O$_4$/CF composites prepared by stirring at room temperature were arranged and distributed in a network. As shown in Figure 2c–f, the prepared material contains the elements Zn, Co, O, and Ni. Experiments show that there are no other impurities in the synthesized products. The similar distribution of elemental Zn and O may indicate specific interactions between them, possibly chemical reactions or physical adsorption. The different distributions observed for the elements Co and Ni may imply that they may have undergone different chemical reaction paths in the samples. This may be due to their different chemical properties or influenced by the sample treatment conditions.
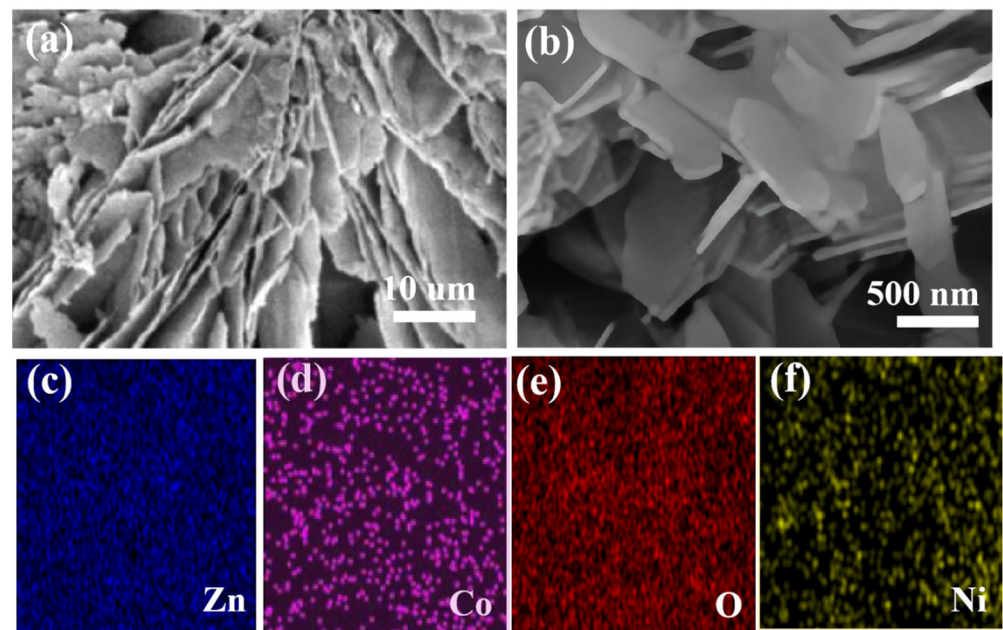

Figure 2. SEM images of (**a**,**b**) Ni-ZnCo$_2$O$_4$/CF materials at different magnifications; (**c**–**f**) mapping of Ni-ZnCo$_2$O$_4$/CF materials.

In order to better observe the microstructure of Ni-ZnCo$_2$O$_4$/CF composites, the microstructure was characterized by transmission electron microscopy. The result is shown in Figure 3. From the inner region of Figure 3a, a clear nanosheet-like structure is visible, and these nanosheets are stacked on top of each other to form pores, which is also consistent with the phenomenon observed in Figure 2. As can be seen from the HRTEM diagram in Figure 3b, the crystal plane spacing of the lattice fringes is 0.23 nm and 0.24 nm, corresponding to the (222) and (311) lattice planes of Ni-ZnCo$_2$O$_4$/CF, respectively. It was found that there are good diffraction rings in the obtained products, indicating that the compounds are polycrystalline.
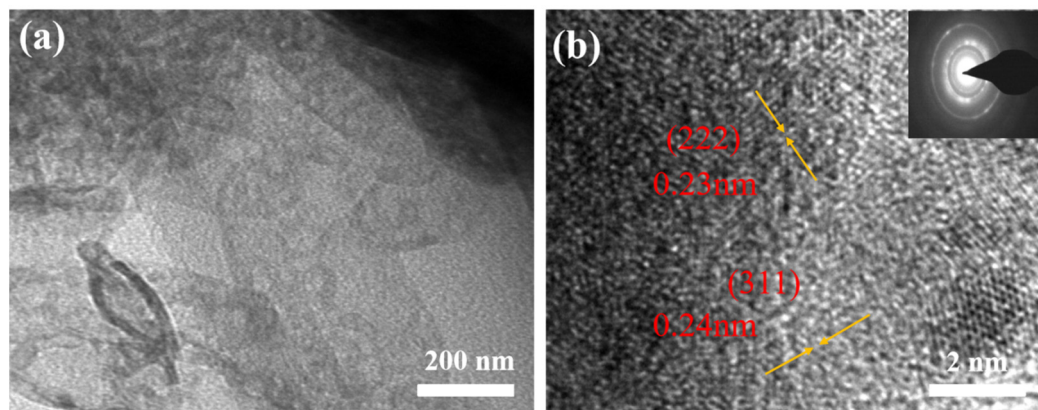
Figure 3. (**a**) TEM image of porous Ni-ZnCo$_2$O$_4$/CF nanomaterials; (**b**) HRTEM image of porous Ni-ZnCo$_2$O$_4$/CF nanomaterials.

Figure 4a presents the X-ray diffraction (XRD) analysis of the Ni-ZnCo$_2$O$_4$/CF composite. The illustration reveals the crystallographic makeup of the Ni-ZnCo$_2$O$_4$/CF material captured via sharply defined and singular diffraction peaks, signifying a high level of crystallization and superior product purity within the prepared sample. These discernible diffraction lineages align well with the cubic ZnCo$_2$O$_4$ spinel structure (JCPDF: 01-1149). Peaks occurring at 2-theta values of 19.06°, 31.48°, 36.96°, 38.8°, 45.04°, 55.66°, 59.76°, and 65.36° correspond to the (111), (220), (311), (222), (400), (422), (511), and (440) crystal facets, respectively [8]. Figure 4b offers an exposition of the Energy-Dispersive Spectroscopy (EDS) findings pertaining to the porous Ni-ZnCo$_2$O$_4$/CF network structure. The data confirm that the structure exclusively comprises Zn, Co, O, and Ni constituents, thereby validating the absence of detrimental impurity elements. The convergence of these outcomes empirically proves the successful doping of Ni element.
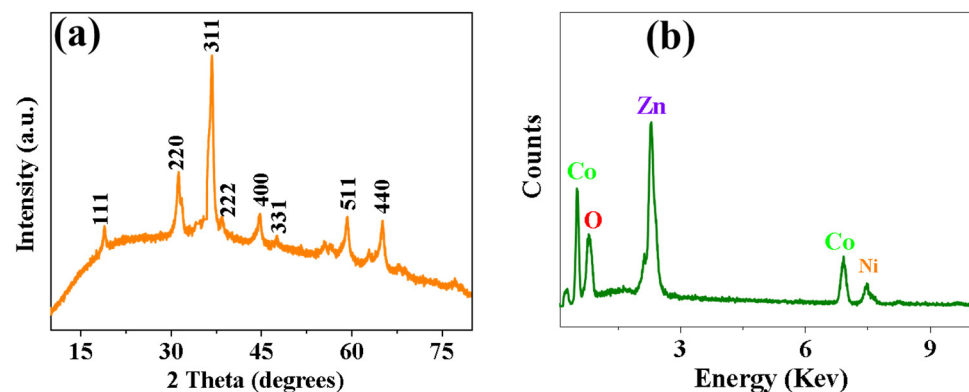

Figure 4. (**a**) XRD patterns of porous Ni-ZnCo$_2$O$_4$/CF nanomaterials; (**b**) EDS spectra of porous Ni-ZnCo$_2$O$_4$/CF nanomaterials.

Figure 5a unveils the cyclic voltammetric curves of the carbon cloth conductive substrate, ZnCo$_2$O$_4$, and Ni-ZnCo$_2$O$_4$/CF, sweeping at a rate of 10 mV·s^{-1}. The confined region by the voltammetry curve for the carbon cloth substrate is notably compact, implying that its specific capacity within the electrochemical reaction procedure is modest and virtually inconsequential. Contrarily, the area encapsulated by the curve for Ni-ZnCo$_2$O$_4$/CF material is impressively expansive, highlighting a significant enhancement in both the specific capacity and charge storage aptitude following the incorporation of Ni elements. Figure 5b delineates the cyclic voltammetry curves of the porous Ni-ZnCo$_2$O$_4$/CF mesh recorded at scan rates of 5, 10, 30, and 50 mV·s^{-1}, within the potential window of −0.2~0.6 V. The figure exhibits that as the scan rate experiences an amplification, there is a proportionate surge in the area cordoned off by the cyclic voltammetric curves, an

indication of an adept charge transfer for the material under investigation. Characteristic oxidation peaks are prominently noticeable nearing the potential window of 0.4 V. At the same time, the emergence of discernible reduction peaks can be observed at the potential window of 0.2 V. These shreds of evidence collectively suggest the occurrence of a redox reaction in the Ni-ZnCo$_2$O$_4$/CF electrode material, signaling a distinctive pseudocapacitive charge–discharge storage mechanism.
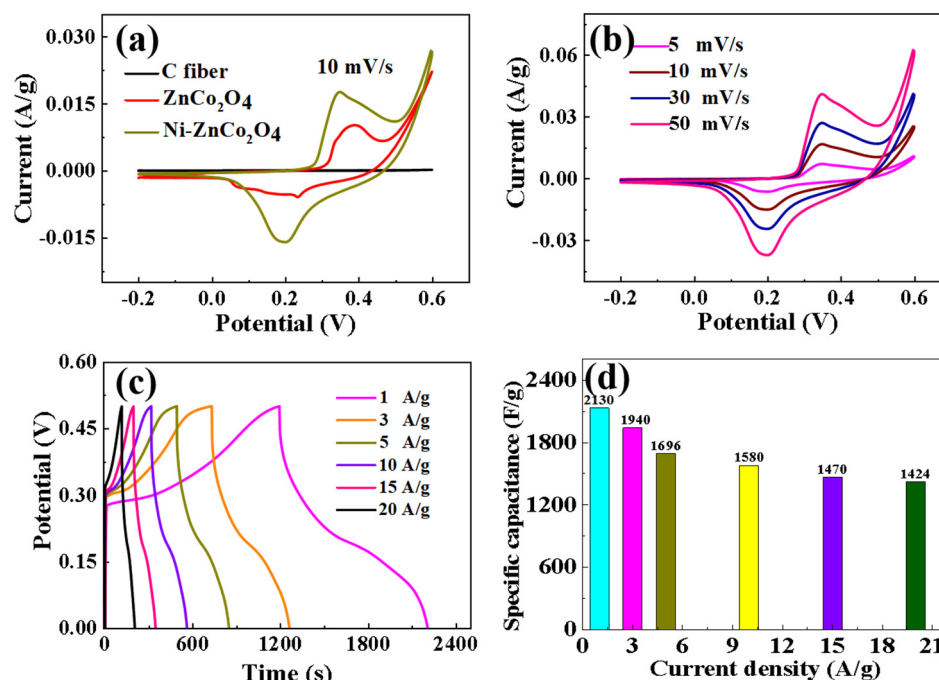

Figure 5. (**a**) Showcases the CV curves of carbon fiber, ZnCo$_2$O$_4$, and Ni-ZnCo$_2$O$_4$/CF, conducted at a scanning speed of 10 mV·s^{-1}. (**b**) Illustrates the CV curves of Ni-ZnCo$_2$O$_4$/CF composites at varying scanning speeds of 5, 10, 30, and 50 mV·s^{-1}. (**c**) Presents the charge/discharge diagrams of Ni-ZnCo$_2$O$_4$/CF composites at assorted current densities. (**d**) Depicts the specific capacitance diagram of Ni-ZnCo$_2$O$_4$/CF composites across multiple current densities.

Figure 5c shows the charging and discharging test results of the Ni-ZnCo$_2$O$_4$/CF material at different current densities. Experiments show that the material has good electrochemical performance during the charge–discharge process, its charge–discharge curve is basically symmetric, and the specific capacitance of the Ni-ZnCo$_2$O$_4$/CF material is calculated based on the charge–discharge curve of the material, as shown in Figure 5d, and the porous Ni-ZnCo$_2$O$_4$/CF electrode material at the current densities of 1, 3, 5, 10, 15, and 20 A·g^{-1}. The specific capacitances were 2130, 1940, 1696, 1580, 1470, and 1424 F·g^{-1}, respectively. The electrochemical properties of Ni-ZnCo$_2$O$_4$ nanomaterials and comparison with references [9–12] are given in Table 2.

Specific surface area and pore size have an important influence on the performance of the material, and we further carried out relevant tests on the material, as shown in Figure 6. Figure 6a,b show the specific surface area curves and pore size distribution curves of ZnCo$_2$O$_4$ material with the values of 99.02 m^2/g and near 30 nm, respectively, and Figure 6c,d show the specific surface area curves and pore size distribution curves of Ni-ZnCo$_2$O$_4$ material with the values of 109.31 m^2/g and near 32 nm, respectively. Comparison reveals that the Ni-ZnCo$_2$O$_4$ material has a larger specific surface area and a richer pore structure. This property enables the electrolyte and electrode materials to come into contact more fully, provides more electrochemical reaction sites, and shortens the electron and ion transport distance, thus increasing the reaction rate and helping to enhance the electrochemical performance of the materials.

Table 2. Comparative Analysis of the Properties of the Electrode Materials Presented in this Study and those Documented in the Literature.

Electrode Material	Current Density/(A/g)	Specific Capacitance/(F/g)	Cycle Number	Capacitance Retention/%	Ref.
Hollow cotton carbon-based $NiCo_2S_4/NiMoO_4$ hybrid arrays	5.0	2323	10,000	90.0	[9]
$OV\text{-}ZnCo_2O_4$	1.0	211.6			[10]
$NiMoO_4/CoMoO_4$ nanorods	1.0	1445	3000	78.8	[11]
$ZnCo_2O_4@NiCo_2O_4$	1.0	1728.1	10,000	91.3	[12]
$Ni\text{-}ZnCo_2O_4$	1.0	2130	10,000	91.8	This paper
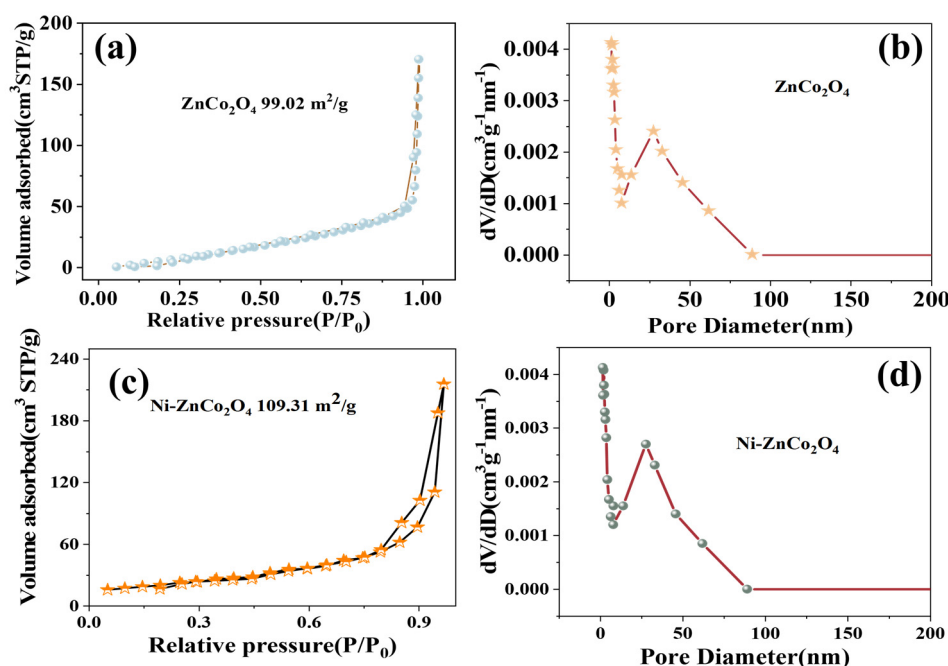
Figure 6. Presents the N_2 adsorption/desorption plots and pore size distribution analyses for both $ZnCo_2O_4$ and $Ni\text{-}ZnCo_2O_4$. Specifically, parts (**a**,**b**) exhibit the N_2 adsorption/desorption trajectories and corresponding pore size dispersal patterns for $ZnCo_2O_4$, respectively. Parts (**c**,**d**), on the other hand, depict the N_2 adsorption/desorption curves and pore size distribution profiles for the Ni-$ZnCo_2O_4$ composite.

Figure 7a shows the impedance curves of $ZnCo_2O_4/CF$ material and $Ni\text{-}ZnCo_2O_4/CF$ material. The curves in the figure consist of high and low frequencies, with the high-frequency region representing the impedance of the ions passing through the surface film of the electrode material and the low-frequency region representing the charge-transfer impedance. In general, the value of the horizontal axis indicates Rs, and its value can be read according to the intercept of the curve and the horizontal axis; it can be seen that the intercept of the $Ni\text{-}ZnCo_2O_4/CF$ material is smaller than that of the $ZnCo_2O_4/CF$ material, which proves that the $Ni\text{-}ZnCo_2O_4/CF$ material has good electrical conductivity. The diameter of the curve similar to a semicircle in the high-frequency region is denoted as Rct, and the value of Rct is correlated with the semicircle diameter; it can be seen in the figure that the radius of the $Ni\text{-}ZnCo_2O_4/CF$ material is smaller than that of the $ZnCo_2O_4/CF$ material, indicating that the $Ni\text{-}ZnCo_2O_4/CF$ has a good charge-transferring ability. Figure 7b illustrates the cyclic stabilization properties of the material at different current densities after repeating 100 cycles. As shown, at a current density of 15 $A·g^{-1}$,

the material has a specific capacitance of 1470 F·g^{-1}. After every 100 changes, the current density was restored to 15 A·g^{-1}, and its specific capacitance was 1456 F·g^{-1}, which was 99.0% of the original specific capacitance. The results show excellent multiplicity performance and cycling stability at different current densities, and the decrease in the specific capacity of the materials is very small, which is due to the fact that a few materials cannot fully participate in the reaction, and a few irreversible changes during the process of current increase.
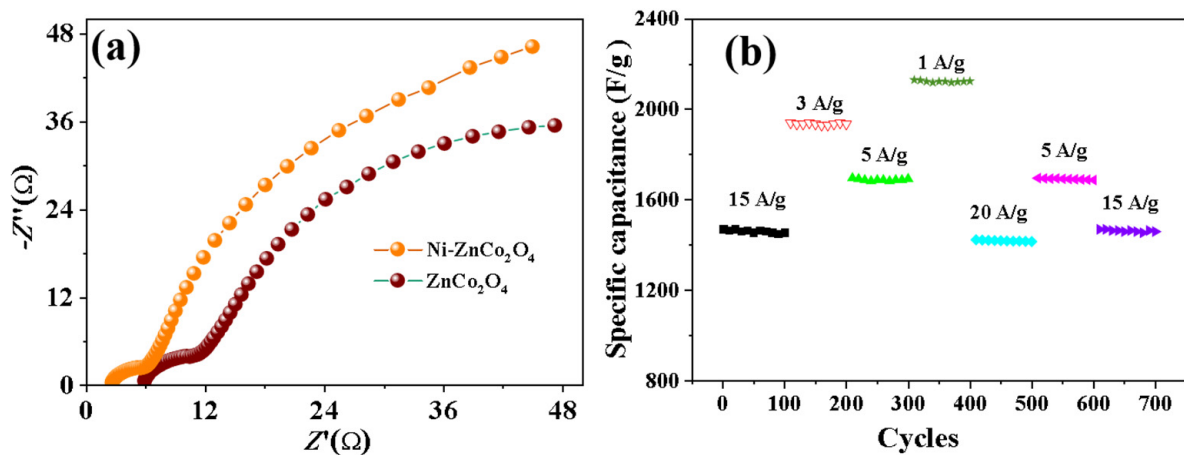

Figure 7. (**a**) Nyquist plots of Ni-ZnCo$_2$O$_4$/CF composites versus ZnCo$_2$O$_4$/CF materials; (**b**) rate and cycling performance of Ni-ZnCo$_2$O$_4$/CF composites at different current densities.

In order to further study the practical application value of Ni-ZnCo$_2$O$_4$/CF composites, we assembled Ni-ZnCo$_2$O$_4$/CF composites//CNTs asymmetric supercapacitors. The Ni-ZnCo$_2$O$_4$/CF composite is the positive electrode, and the CNTs are the negative electrode, because the carbon nanotubes have a very high specific surface area, which means that more surface area is available for charge storage per unit mass or per unit volume, and they have excellent electrical conductivity, which enables them to transport electrons quickly, thus reducing the charge transport impedance and improving the charge and discharge speeds and performance of the supercapacitor [13,14]. A schematic diagram of the supercapacitor structure is shown in Figure 8.
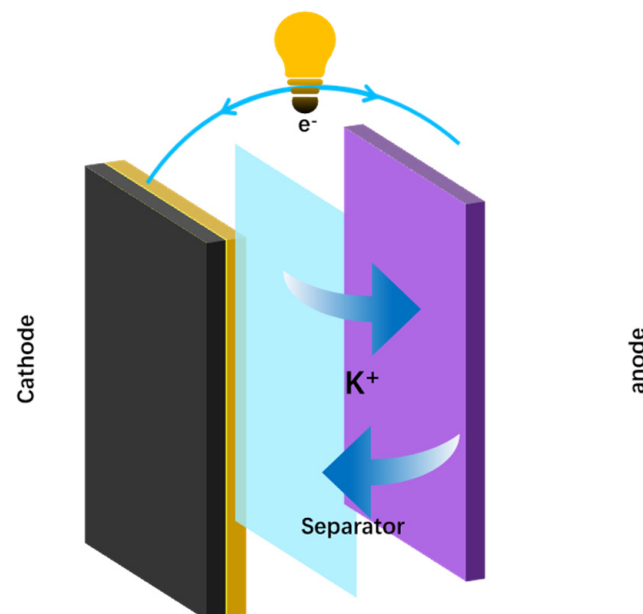

Figure 8. Schematic diagram of the working principle of the supercapacitor device.

First, the experiment was conducted to test the negative electrode material to explore the electrochemical performance of this material under different currents, as shown in Figure 9. Figure 9 shows the charging/discharging curves of CNTs electrodes at different current densities. The constant-current charging and discharging curves are triangularly symmetric, indicating good reversibility of charging and discharging. The specific capacities of the CNTs electrodes were calculated as 262, 238, 218, 184, 162, and 152 $F \cdot g^{-1}$ based on the discharge curves at current densities of 1, 3, 5, 10, 15, and 20 $A \cdot g^{-1}$, respectively.
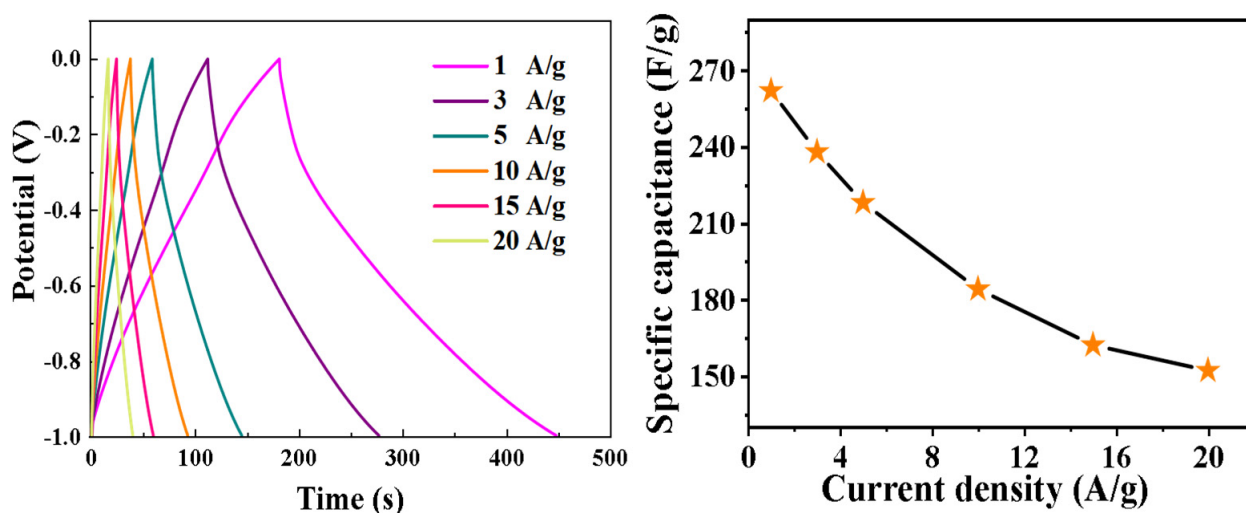
Figure 9. Charge/discharge curves of carbon nanotube electrodes at different current densities and corresponding specific capacities.

Figure 10a unfolds the comparative CV curves for the electrode materials of carbon nanotubes (CNTs) and nickel-zinc cobaltate (Ni-ZnCo$_2$O$_4$/CF). The Ni-ZnCo$_2$O$_4$/CF//CNTs asymmetric supercapacitor device was constructed utilizing Ni-ZnCo$_2$O$_4$ and carbon nanotubes as electrode materials. Specifying Ni-ZnCo$_2$O$_4$/CF as the positive electrode and carbon nanotubes as the negative electrode, the disparity amidst the positive and negative potential windows was employed as the voltage span. Upon computation, a theoretical potential window of 1.6 V was derived. Figure 10b portrays the cyclic voltammetry curves subsisting under varying voltage windows. These curves maintain a roughly congruous form across different voltage windows, confirming the commendable reversibility of the device. Figure 10c delineates the CV plot for the Ni-ZnCo$_2$O$_4$/CF//CNTs apparatus at assorted scan rates, within the voltage window range of 0–1.6 V. Conversely, Figure 10d showcases the CV profile of the identical device. As the scanning rate escalates, the area within the curve witnesses an enlargement, albeit the general form remains inherently stable, indicating impressive steadiness. Figure 10d also highlights the charge–discharge plots for the Ni-ZnCo$_2$O$_4$/CF//CNTs at fluctuating current densities, with the results manifesting commendable electrochemical reversibility of the material. As depicted in Figure 10e, cycle stability tests were conducted on the Ni-ZnCo$_2$O$_4$/CF//CNTs devices, where the specific capacitance attenuated from the initial 182 $F \cdot g^{-1}$ to 167 $F \cdot g^{-1}$ following 10,000 testing cycles at a current density of 1 $A \cdot g^{-1}$, yielding a cycle stability of 91.8%. The experimental outcomes thereby substantiate the admirable cycle stability and longevity of the electrode material. Lastly, Figure 10f compares the energy density and power density of the device against other energy storage devices [12,15–17]. This device stands out, with a paramount energy density of 73.4 Wh/kg and a power density of 923 W/kg. This competitive edge makes the device fabricated in this research significantly superior to its peers in the field, as referred to in the pertinent literature.
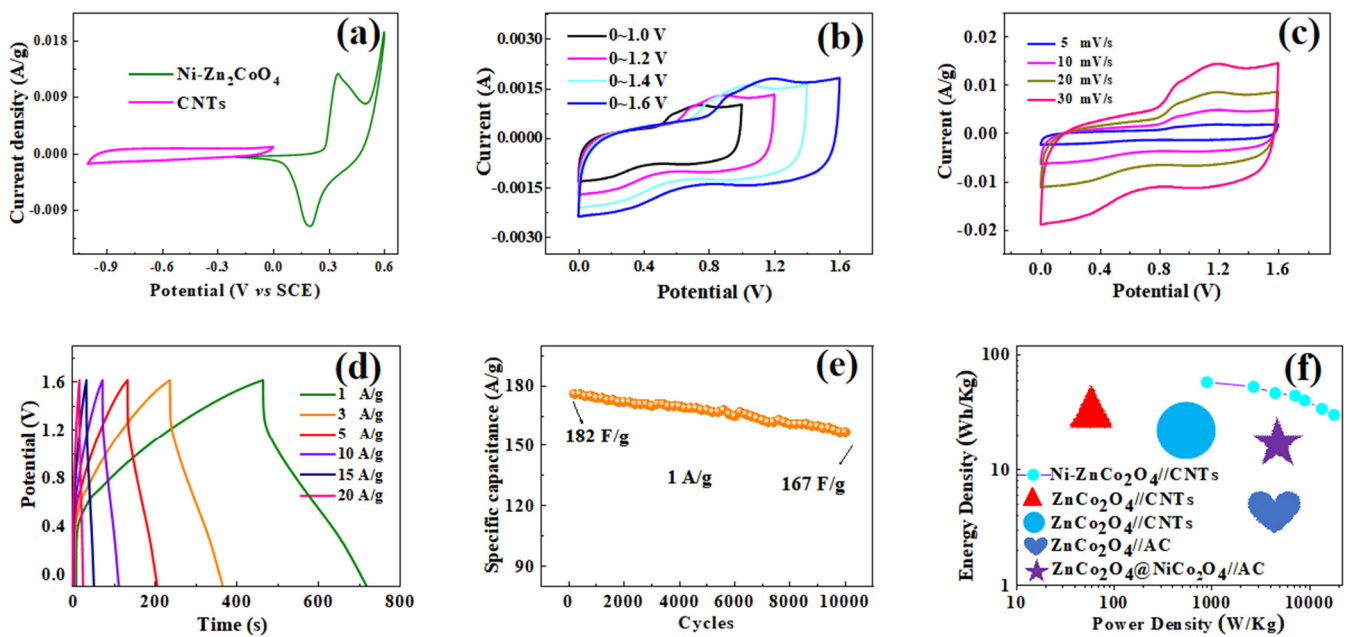
Figure 10. (**a**) CV curves of Ni-ZnCo$_2$O$_4$/CF and CNTs electrodes; (**b**) CV curves of Ni-ZnCo$_2$O$_4$/CF//CNTs devices at different potential windows; (**c**) CV profiles of Ni-ZnCo$_2$O$_4$/CF//CNTs devices at different scan rates; (**d**) Charge and discharge curves of Ni-ZnCo$_2$O$_4$/CF//CNTs devices at different current densities; (**e**) Performance of Ni-ZnCo$_2$O$_4$/CF//CNTs devices at 10,000 cycles at 1 A·g^{-1} current density; (**f**) Comparison between Ni-ZnCo$_2$O$_4$/CF//CNTs devices and other devices (See Refs. [12,15–17]).

4. Conclusions

In this paper, nickel-element-doped zinc cobaltate/carbon fiber composites were prepared on a carbon cloth substrate composed of carbon fibers by using a simple room-temperature stirring method combined with heat treatment, and the samples have the advantages of porous network structure, high purity, and high cycling performance. The electrochemical properties of the Ni-ZnCo$_2$O$_4$/CF electrode materials were investigated. The electrode has a specific capacitance of 1470 F·g^{-1} at a current density of 15 A·g^{-1} and is able to maintain a specific capacity of 99.0% for every 100 changes in current density. The Ni-ZnCo$_2$O$_4$/CF//CNTs device was subjected to 10,000 charge/discharge tests at a current density of 1 A·g^{-1}, and its specific capacity stability reached 91.8%. The above experiments proved that the electrode material exhibited better cycle stability and cycle life during the charge–discharge process.

Author Contributions: D.C., Y.L., J.W. (Jun Wang) and T.M. carried out the experiments and wrote the manuscript, and J.W. (Jing Wang) designed this experiment and wrote the manuscript and other analyses. H.Z., W.X. and Y.W. carried out the characterization tests, analyzed, and wrote the results. All authors have read and agreed to the published version of the manuscript.

Institutional Review Board Statement: Not applicable.

Informed Consent Statement: Not applicable.

Data Availability Statement: Data are contained within the article.

Conflicts of Interest: The authors declare no conflict of interest.

References

1. Rahman, A.; Farrok, O.; Haque, M.M. Environmental impact of renewable energy source based electrical power plants: Solar, wind, hydroelectric, biomass, geothermal, tidal, ocean, and osmotic. *Renew. Sustain. Energy Rev.* **2022**, *161*, 112279. [CrossRef]
2. Wang, M.; Jiang, C.; Zhang, S.; Song, X.; Tang, Y.; Cheng, H. Reversible calcium alloying enables a practical room-temperature rechargeable calcium-ion battery with a high discharge voltage. *Nat. Chem.* **2018**, *10*, 667–672. [CrossRef] [PubMed]
3. Sinha, P.; Kar, K.K. Introduction to supercapacitors. In *Handbook of Nanocomposite Supercapacitor Materials II: Performance*; Springer International Publishing: Cham, Switzerland, 2020; pp. 1–28.
4. Li, M.; Guo, Q.; Chen, L.; Li, L.; Hou, H.; Zhao, Y. Microstructure and properties of graphene nanoplatelets reinforced AZ91D matrix composites prepared by electromagnetic stirring casting. *J. Mater. Res. Technol.* **2022**, *21*, 4138–4150. [CrossRef]
5. Zhao, Y. Stability of phase boundary between L1$_2$-Ni$_3$Al phases: A phase field study. *Intermetallics* **2022**, *144*, 107528. [CrossRef]
6. Balaji, T.E.; Tanaya Das, H.; Maiyalagan, T. Recent trends in bimetallic oxides and their composites as electrode materials for supercapacitor applications. *ChemElectroChem* **2021**, *8*, 1723–1746. [CrossRef]
7. Javed, M.S.; Khan, A.J.; Ahmad, A.; Siyal, S.H.; Akram, S.; Zhao, G.; Bahajjaj, A.A.A.; Ouladsmane, M.; Alfakeer, M. Design and fabrication of bimetallic oxide nanonest-like structure/carbon cloth composite electrode for supercapacitors. *Ceram. Int.* **2021**, *47*, 30747–30755. [CrossRef]
8. Zhou, G.; Zhu, J.; Chen, Y.; Mei, L.; Duan, X.; Zhang, G.; Chen, L.; Wang, T.; Lu, B. Simple method for the preparation of highly porous ZnCo$_2$O$_4$ nanotubes with enhanced electrochemical property for supercapacitor. *Electrochim. Acta* **2014**, *123*, 450–455. [CrossRef]
9. Ren, B.; Zhang, X.; An, H.; Ding, S.; Zhang, H.; Zeng, X.; Fan, M.; Yang, X. Hollow cotton carbon based NiCo$_2$S$_4$/NiMoO$_4$ hybrid arrays for high performance supercapacitor. *J. Energy Storage* **2023**, *59*, 106553. [CrossRef]
10. Xiang, K.; Wu, D.; Fan, Y.; You, W.; Zhang, D.; Luo, J.L.; Fu, X.Z. Enhancing bifunctional electrodes of oxygen vacancy abundant ZnCo$_2$O$_4$ nanosheets for supercapacitor and oxygen evolution. *Chem. Eng. J.* **2021**, *425*, 130583. [CrossRef]
11. Nti, F.; Anang, D.A.; Han, J.I. Facilely synthesized NiMoO$_4$/CoMoO$_4$ nanorods as electrode material for high performance supercapacitor. *J. Alloys Compd.* **2018**, *742*, 342–350. [CrossRef]
12. Wu, Z.; Yang, X.; Gao, H.; Shen, H.; Wu, H.; Xia, X.; Wu, X.; Lei, W.; Yang, J.; Hao, Q. Controllable synthesis of ZnCo$_2$O$_4$@NiCo$_2$O$_4$ heterostructures on Ni foam for hybrid supercapacitors with superior performance. *J. Alloys Compd.* **2022**, *891*, 162053. [CrossRef]
13. Wang, T.; Chen, H.C.; Yu, F.; Zhao, X.; Wang, H. Boosting the cycling stability of transition metal compounds-based supercapacitors. *Energy Storage Mater.* **2019**, *16*, 545–573. [CrossRef]
14. Wu, Q.; He, T.; Zhang, Y.; Zhang, J.; Wang, Z.; Liu, Y.; Zhao, L.; Wu, Y.-Z.; Ran, F. Cyclic stability of supercapacitors: Materials, energy storage mechanism, test methods, and device. *J. Mater. Chem. A* **2021**, *9*, 24094–24147. [CrossRef]
15. Wu, L.; Sun, L.; Li, X.; Zhang, Q.; Si, H.; Zhang, Y.; Wang, K.; Zhang, Y. Mesoporous ZnCo$_2$O$_4$-CNT microflowers as bifunctional material for supercapacitive and lithium energy storage. *Appl. Surf. Sci.* **2020**, *506*, 144964. [CrossRef]
16. Lu, Y.; Wang, L.; Chen, M.; Wu, Y.; Liu, G.; Qi, P.; Fu, M.; Wu, H.; Tang, Y. Rationally designed hierarchical ZnCo$_2$O$_4$/C core-shell nanowire arrays for high performance and stable supercapacitors. *J. Alloys Compd.* **2021**, *876*, 160037. [CrossRef]
17. Bhagwan, J.; Hussain, S.K.; Yu, J.S. Aqueous asymmetric supercapacitors based on ZnCo$_2$O$_4$ nanoparticles via facile combustion method. *J. Alloys Compd.* **2020**, *815*, 152456. [CrossRef]